Available online at www.sciencedirect.com
ScienceDirect
International Journal of Heat and Mass Transfer 50 (2007) 1879–1891
International Journal of HEAT and MASS TRANSFER
www.elsevier.com/locate/ijhmt

Pressure drop studies on two-phase flow in a uniformly heated vertical tube at pressures up to the critical point

B.R. Vijayarangan, S. Jayanti, A.R. Balakrishnan *

Department of Chemical Engineering, Indian Institute of Technology Madras, Chennai 600 036, India

Received 11 May 2006; received in revised form 29 September 2006
Available online 20 December 2006

Abstract

Measurements of two-phase flow pressure drop have been made during a phase-change heat transfer process with refrigerant (R-134a) as a working fluid for a wide range of pressures right up to the critical pressure. The experiments were conducted in a uniformly heated vertical tube of 12.7 mm internal diameter and 3 m length over a heat flux range of 35–80 kW/m^2, mass flux range of 1200–2000 kg/m^2 s, exit quality range of 0.19–0.81 and for reduced pressures ranging from 0.24 to 1 with a fixed inlet subcooling of 3 °C. The measurements were compared with the predictions from the homogeneous flow model, a separated flow model using correlations drawn from the literature for void fraction and frictional pressure drop, and finally, using a flow pattern-based predictive method accounting specifically for bubbly, slug and annular flow regimes. It was found that the best results were obtained with the flow pattern-based approach with a mean deviation of ±20% over the entire pressure range.

1. Introduction

The knowledge of two-phase pressure drop over the wide range of system pressures is important in design and development of compact heat exchangers, nuclear reactors and cryogenic and refrigeration equipment. In gas–liquid two-phase flow through a vertical pipe, the pressure gradient consists of three components: friction, acceleration and hydrostatic, and the overall pressure gradient is written as (Collier [1])

$$\frac{dp}{dz} = \frac{dp_f}{dz} + \frac{dp_a}{dz} + \frac{dp_h}{dz} \quad (1)$$

Here, the frictional component arises due to viscous friction at the walls and is a strong function of the flow velocities and the characteristic flow patterns or flow regimes that the gas–liquid flow assumes within the tube. The gravitational component is a strong function of the void fraction or the fractional volume occupied by the gas phase within the tube which itself is a function of the flow conditions. The acceleration component depends both on the quantity of vapour and liquid flowing through the pipe (which can vary along the length in a heated tube) as well as on the radial profiles of the velocities of the phases. In general, all the three components are influenced by a range of geometric and flow parameters as well as the thermophysical properties of the media flowing through the tube. A large number of systematic studies, starting with the early work of Lockhart and Martinelli [2], have been carried out over the past several decades. It was recognized early on (Baker [3]) that the distribution of the two phases within the cross-section assumes characteristic shapes called flow patterns or flow regimes. A number of flow pattern maps have been developed (see [4] for a review) to predict the conditions under which a particular flow regime prevails. Effort has been made to develop "phenomenological" models for specific flow regimes such as slug flow [5–7] and annular flow [8,9] to predict the hydrodynamic characteristics of these flow regimes. Simultaneously, a number

* Corresponding author. Tel.: +91 44 2257 4154; fax: +91 44 2257 0509.
E-mail address: arbala@iitm.ac.in (A.R. Balakrishnan).

0017-9310/$ - see front matter © 2006 Elsevier Ltd. All rights reserved.
doi:10.1016/j.ijheatmasstransfer.2006.10.018

of empirical correlations have been developed for the prediction of void fraction and pressure drop [10–12]. In addition, theoretical models based on idealization of the flow such as the homogeneous flow and the separated flow [1] have also been proposed.

There is thus a vast amount of literature on the prediction of pressure drop in gas–liquid flow in a tube. Nearly all prediction methods require experimental information to a varying degree. Purely empirical models such as those of Lockhart and Martinelli [2], Chisholm [13] and Friedel [12] are dependent wholly on empirical information for both frictional pressure gradient and void fraction. Flow pattern based models such as those for slug flow and annular flow require, in addition to flow pattern transition criteria, more detailed data which enable the models to reconstruct the hydrodynamics. Thus, the slug flow model of Orell and Rembrand [14] for vertical flow requires information on the slug length, slug frequency etc. This empirical information is then used along with fundamental mass and momentum conservation equations and other kinematic and constitutive conditions to arrive at an overall flow model which enables the calculation of the pressure gradient and void fraction. Similarly, the annular flow model of Hewitt and Govan [9] requires empirical input of entrainment and redeposition rates of the liquid droplets and effective roughness of the interfacial waves in order to calculate the overall film thickness and pressure gradient. Often, this crucial information, which in many cases is necessary for accuracy in predictions, is obtained from adiabatic air–water experiments at relatively low pressures. The overall model is then validated by comparing with experimental data of integral parameters such as the pressure drop over a length of tube and location of dryout etc. A case in point is the annular flow model which was originally developed based on adiabatic air–water data but which has since been applied successfully to non-adiabatic systems at pressures up to 70 bar [9]. However, recent studies [15,16] have shown that extension of the model to much higher pressures (say, greater than 100 bar for a steam–water system) was not straightforward and that correction factors for both entrainment and deposition rates had to be incorporated to obtain good results.

Clearly, there is a need for experimental data at high system pressures for validation and extension of the current models for thermal hydraulics of a vapour generating tube. Several flow boiling studies have been conducted recently in tubes of small diameters including in systems other than steam and water. However, most of these studies have been for horizontal tubes [17–22] and contain their own correlations based on modifications of existing correlations. Thus, Tran et al. [17], Warrier et al. [22] and Yu et al. [20] proposed modifications to the correlation of Chisholm [13]); Zhang and Ralph [19] proposed a modification to the correlation of Friedel [12]; and Sony and Comeau [21] proposed a correlation for the two-phase multiplier [1].

Some pressure drop studies have also been carried out for flow in vertical tubes. Fu and Klausner [23] presented an annular flow-based model for the prediction of pressure drop in an evaporating tube and compared their model predictions with essentially near-atmospheric pressure data taken from the literature covering up, down and microgravity flow conditions. They found satisfactory agreement with their flow pattern-based model. Tong et al. [24] conducted pressure drop experiments under single phase and subcooled flow boiling conditions of water flowing through channels in the diameter range of 1 and 2.5 mm at system pressures ranging from 4 to 16 bar and for mass fluxes in the range of 25,000–45,000 kg/m^2 s. They found the length-to-diameter ratio to be a significant parameter in determining the pressure drop and presented separate correlations for pressure drop for single phase and subcooled flow boiling conditions. Zhao and Bi [25] measured the pressure drop in small triangular vertical channels under air–water flow conditions and showed that the Lockhart and Martinelli [2] approach would be accurate if the single phase friction factor through the small channels was calculated using the correlation of Churchill [26]). Chen et al. [27] developed a homogeneous model-based correlation for the frictional pressure gradient in a small diameter tube using air–water data from the literature including data from microgravity experiments. Wen and Kenning [28] investigated two-phase pressure drop during flow boiling of water in a vertical channel of 2 mm by 1 mm cross-section at near-atmospheric pressures. They performed experiments for the conditions of heat flux from 25 to 105 kW/m^2, mass flux from 57 to 211 kg/m^2 s and exit quality from 9% to 30%. They compared their data with a number of correlations and presented a modified correlation based on the Lockhart–Martinelli model [2].

The available literature on measurement and prediction of pressure drop under flow boiling conditions falls short on two counts: lack of data at high pressures, especially in the diameter range of 10–20 mm, and the use of purely empirical approach to the prediction of the two-phase flow pressure drop. These two aspects are simultaneously addressed in the present study wherein experimental data are reported for flow boiling of R-134a in a vertical tube of 12.5 mm inner diameter for system pressures up to a reduced pressure (working pressure/critical pressure) of 0.95. The results are then used to validate a flow pattern-based estimate of the pressure drop in the pipe. Details of the investigation and the results are discussed below.

2. Experimental set-up

The test rig used in the present investigation was designed and fabricated to study two-phase pressure drop, boiling heat transfer and CHF with the refrigerant R-134a as the working fluid flowing in a closed loop system. The schematic diagram of the experimental set-up is shown in Fig. 1. The test rig consists of the primary loop, the chilling unit loop, the cooling water loop and the data acquisition system. These are described below.

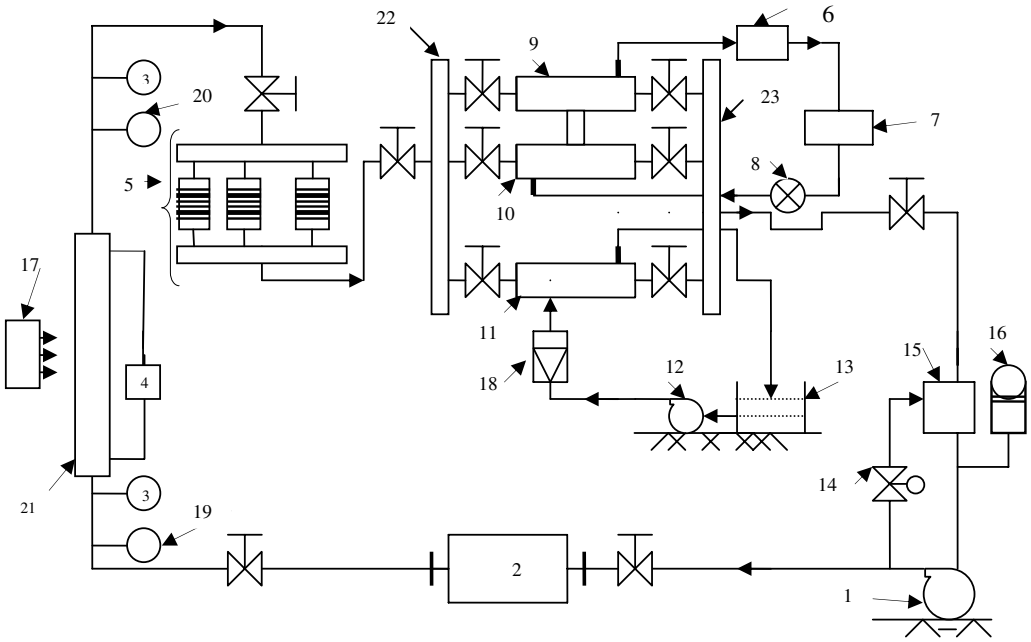

1. Refrigerant circulating pump
2. Mass flow meter
3. Absolute pressure transducer
4. Differential pressure transducer
5. Pressure regulating valves
6. Compressor
7. Condenser
8. Expansion valve
9. Low temperature condensers (-30 °C to 0 °C)
10. Low temperature condensers (0 °C to +30 °C)
11. Water cooled condenser
12. Water circulating pump
13. Temperature controlled water tank
14. By-pass valve
15. Receiver tank
16. Piston type accumulator
17. D.C. rectifier
18. Rotameter
19. Inlet temperature indicator
20. Outlet temperature indicator
21. Test section
22. Inlet header
23. Outlet header

Control valves

Fig. 1. Schematic diagram of test loop.

2.1. Primary loop

In this loop the working fluid, R-134a, flows in a closed path. It consists of a refrigerant pump, an accumulator, a mass flow meter, the test section, a filter, pressure transducers, a pressure regulating valve and a receiver tank. The refrigerant is circulated through the loop by a hermetically sealed oil-free canned motor pump. A piston type accumulator is used to increase and maintain the desired pressure level of the loop. A calibrated micromotion mass flow meter (R-series) is used to measure the mass flow rate at the delivery of the pump. A flow and pressure-regulating valve is positioned in between the mass flow meter and the pump. The required flow rate at the test section can be achieved by operating the main and the bypass valve provided at the pump delivery. The vertically up flow test section (see below), is positioned after the mass flow meter as shown in Fig. 1. The liquid–vapour mixture from the

test section passes through the cooling loop and the condensed liquid is fed to the receiver tank connected to the suction end of the pump.

2.2. Chilling unit loop

The chilling unit loop is another closed loop system, which enables the R-134a system to be operated at pressures as low as 5 bar and as high as the critical pressure (40.56 bar). It contains three condensers connected in parallel and designed to work at different pressure and temperature ranges. The first condenser works in the temperature range of +30 to +100 °C (corresponding to test section pressure range of 7 and 40.56 bar) and uses tap water as the heat sink. The second and the third condensers are designed to operate in the temperature ranges of 0–30 °C and −30 to 0 °C, respectively corresponding to test section pressure ranges of 3–7 bar and 1 and 3 bar, respectively. These two condensers form a closed loop with a refrigerant mixture of R-12 and R-404a providing the heat sink to the primary coolant. The chilling unit loop is equipped with an open type air-cooled and hermetically sealed oil-cooled compressor with a common intercooler to circulate the refrigerant mixture through the condenser units. The condensers are of shell-and-tube type of heat exchangers in which R-134a flows on the tube side and R-12 and R-404a mixture on the shell side. Depending on the operating pressure and temperature of the primary system, only one of the condensers is operated at any time.

2.3. Cooling water loop

The third condenser works with cooling water on the shell side and the refrigerant R-134a on the tube side. The cooling water is circulated through a 3 HP pump. The required flow rate of the cooling water can be set by adjusting the main valve and the bypass valve. The flow rate is measured by a rotameter positioned on the delivery side of the pump. The inlet and the outlet temperatures of the cooling water are measured using T-type thermocouples.

The entire closed loop of the test rig was subjected to a hydrostatic pressure test up to 60 bar to ensure 100% leak-free operation at 40 bar with R-134a. Before filling up the rig with R-134a, a fine vacuum of the order of 0.1 Pa was created using a direct driven vacuum pump to ensure proper filling of the refrigerant.

2.4. Test section

The test section is made of stainless steel (SS-304) and has an inner diameter of 12.7 mm and an outside diameter of 16.7 mm. The heated length of the test section is 3 m. A low voltage, high current DC power supply (maximum rating 17 V DC, 800 A) is used to heat the test section. The DC power is supplied through two copper bus bars of 100 mm width and 7 mm thickness connected across the test section length of 3 m. The test section is well-insulated with asbestos rope and polyurethylene foam to minimize heat losses to the surroundings.

Details of the instrumentation on the test section are shown in Fig. 2. The bulk fluid temperature is measured at the inlet (T_{in}), at the outlet (T_{out}) of the test section and at five other intermediate locations using mineral insulated T-type thermocouples of 1.10 mm outside diameter. The wall temperature of the test section is measured at 40 axial locations along the heated length using T-type thermocouples of bead diameter of 0.8 mm. All the thermocouples are isolated from any disturbance signals from the DC

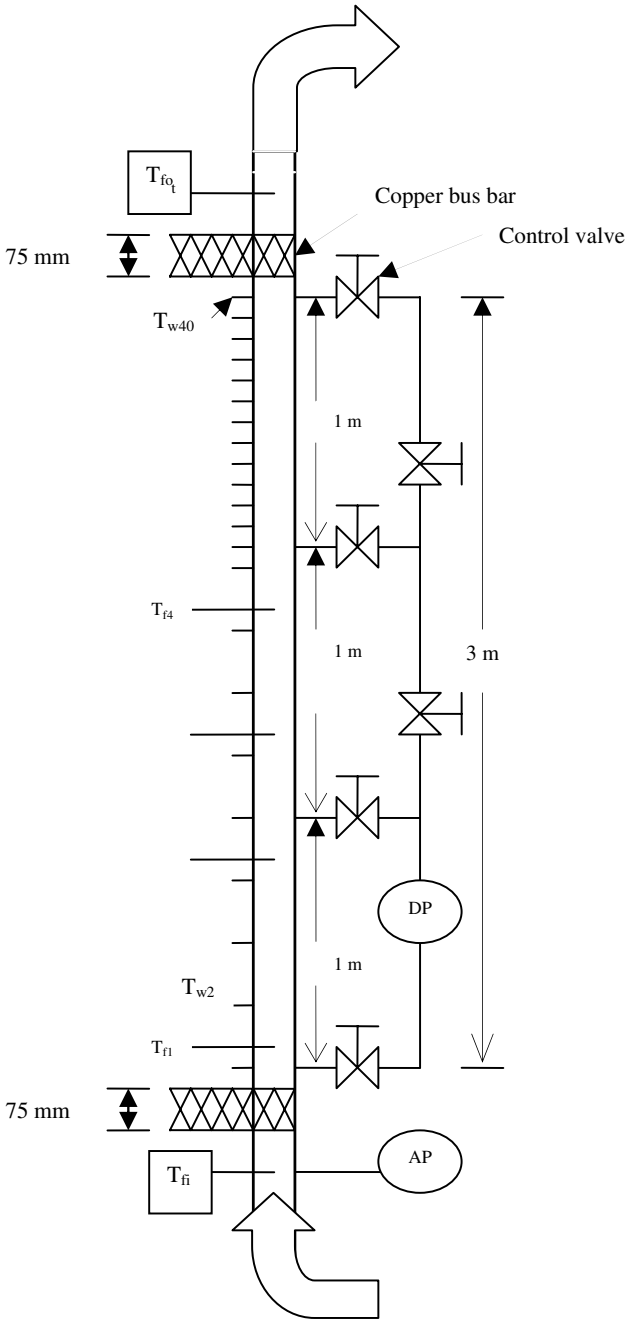

Fig. 2. Test section details.

power supply by a Galvanical signal isolator. This enables the correct measurement of temperature from all these thermocouples. The thermocouples (wall and bulk fluid) were calibrated before installation as well as *in situ*. The nominal accuracy of each thermocouple is 0.1 °C.

A differential pressure transducer is used to measure the pressure drop across the test section length of 3 m. (Measurement over a shorter length of 1 m was also possible; however, this option was not used.) In addition, absolute pressure transducers are located at the test section inlet and at the outlet. All the pressure transducers are connected to the test section through pressure tappings of 1.6 mm diameter. The pressure transducers are electrically isolated by providing teflon seating and bushes in-between the flanges and bolts to which the transducers are connected and have been calibrated with an uncertainty of ±0.25% of the full scale value.

2.5. Data acquisition system

A Contec-made ADI12 PC and an ATP M3 type analog-to-digital add-on cards are used to process ±5 V DC from the measuring instruments and all the millivolt (mV) signals from all thermocouples, respectively. A data acquisition code which includes all calibration equations and conversions to desired engineering units, is used to provide on-screen display of analog signals from all the sensors. The sensor output voltages are time-averaged for the mean quantities of pressure, temperature and flow rates. As a check on steady state, three data sets are compared for consistency before all the scans are averaged together for further processing. The end result is a set of measurements, each an average of 10 readings, and a confirmation of steady state system operation during the collection of data. Signals from all the sensors are processed through a data acquisition system consisting of a PC and a multiplexer and the output is stored on the hard disk of the computer.

2.6. Experimental procedure

In a typical experiment, R-134a from the storage tank is circulated first under subcooled liquid conditions through the test section and the rest of the loop with the help of the hermetic (canned motor) pump. The valves connecting the pressure tapping lines to the test section are also opened so that any vapour present in them is removed. Heat is applied to the test section and the pressure is set to the desired value at the test section. The pressure in the test loop is adjusted by turning on the piston accumulator. Once the system is stabilized at the desired inlet temperature, mass flux, heat flux and pressure, the readings from the differential pressure transducer, the absolute pressure transduser, the inlet and the outlet thermocouples and the mass flow meter are recorded using the data acquisition system. These experiments are repeated for a different flow and pressure conditions. The temperature of the fluid at inlet to the test section is maintained by controlling the temperature and the mass flow rate of cooling water flowing through the heat exchangers. The mass flow rate is regulated by means of control valves. The experiments were conducted in the nominal test section of 12.7 mm diameter with a pressure range of 10–39.7 bar (corresponding reduced pressures in the range of 0.24–0.99), over a mass flux range of 1000–2000 kg/m^2 s and at three heat fluxes values, viz., 35, 60 and 80 kW/m^2. Typically, the lowest heat flux was such that dry out rarely occurred in the tube while the highest heat flux resulted in a significant section of the tube being in the post-dryout regime. The exit quality ranged from 0.10 to 0.87 for the combination of flow parameters. The inlet subcooling was maintained at 3 °C for all cases.

As part of the commissioning of the experimental set-up, instrumentation and data acquisition, single-phase (liquid only) pressure drop experiments were conducted over a range of Reynolds numbers. These data agreed to within ±10% with the Blasius type of correlation for the friction factor.

3. Results from the experiments

The total pressure difference between two points separated by a height of 3 m was measured for different flow conditions. The measured pressure difference included the three components contributing to the pressure change within the test section, namely, the frictional, the accelerational and the gravitational components, as well as the pressure change due to the liquid column in the pressure tapping lines connected to the transducer. The pressure drop in the test section is therefore obtained as follows:

$$\Delta P_{\text{test section}} = \Delta P_{\text{measured}} + \rho_{\text{l}} g H$$

where ρ_{l} is the density of the saturated liquid at the test section pressure and H is the height difference between the pressure taps, which is 3 m in the present case. The measured variation of the pressure drop in the test section with mass flux and pressure is summarized in Fig. 3. Here the measured pressure drop is plotted as a function of the reduced pressure for mass fluxes of 1200, 1400, 1600, 1800 and 2000 kg/m^2 s for a constant wall heat flux of 35 kW/m^2 (Fig. 3a) and 60 kW/m^2 (Fig. 3b). It is seen that the pressure drop decreases nearly linearly with increasing pressure. One interpretation of this is that as the pressure increases for a fixed mass and heat fluxes, the exit quality increases (due to reduced latent heats of vapourization at high pressures), thus increasing the voidage in the tube. This reduced gravitational head which would then result in a lower pressure drop. However, a more detailed analysis (discussed later) shows that all the three components of pressure drop are affected by changes in the system pressure and that no single factor can be attributed to this. The data of Fig. 3 are replotted in terms of the exit quality in Fig. 4. Generally speaking, the high exit quality data refer to the combination of high system pressure and low

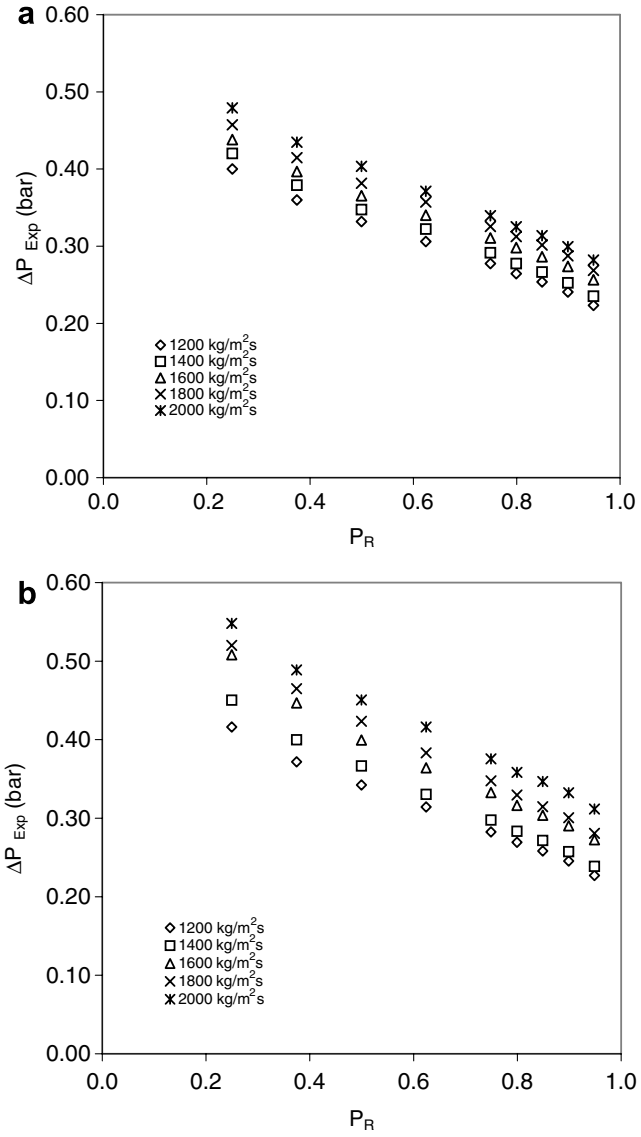

Fig. 3. Measured pressure drop data as a function of reduced pressure for different mass flux and for heat flux of 35 and 60 kW/m^2.

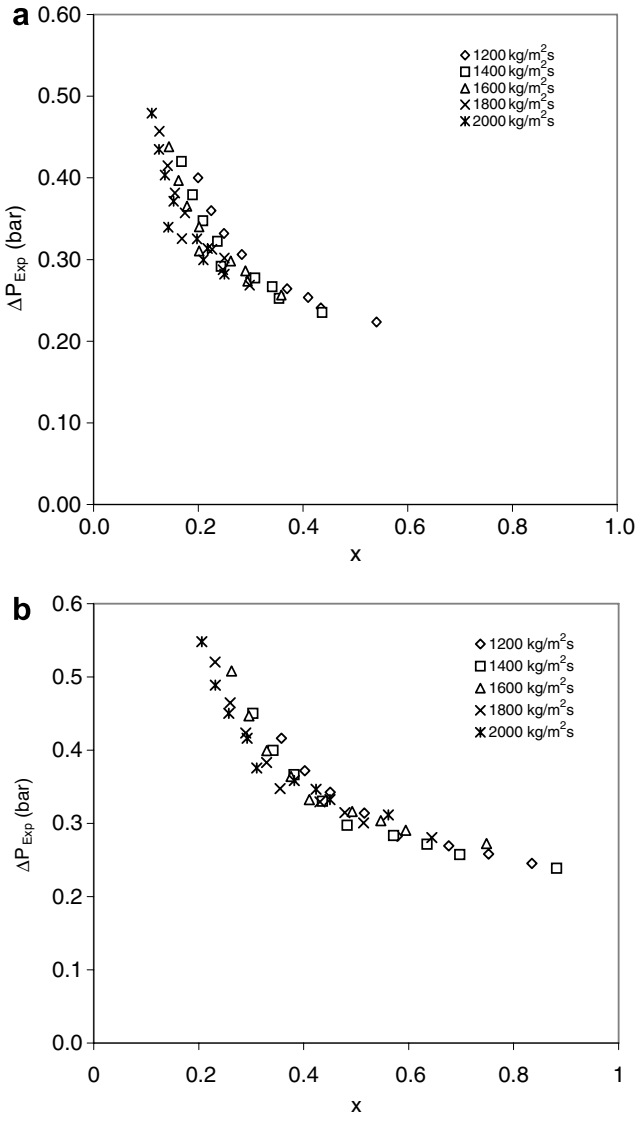

Fig. 4. Measured pressure drop data as a function of quality for different mass flux for heat flux of 35 and 60 kW/m^2.

mass flux. Both factors tend to reduce the pressure gradient.

The data collected in the present study are reported in Table 1. The analysis of these data using conventional empirical correlations and using a flow pattern-based approach are discussed below.

4. Analysis of the pressure drop data

The data obtained in the present study have been analyzed in two ways: firstly, using conventional two-phase flow models and secondly, using a flow pattern-based model. In each case, the overall test section is divided into a number of segments (typically 20) and the pressure drop due to the three components, viz., frictional, gravitational and accelerational components, is estimated. This is then used to calculate the overall test section pressure drop. Since the flow quantities such as the pressure, the phasic flow rates vary along the length of the tube and since these have a strongly non-linear relationship with pressure drop, this segmented approach is expected to give more accurate results than an approach based on only the inlet and the exit conditions.

Two conventional methods have been used to estimate the pressure drop components. In the first method, a homogeneous flow assumption is made. This enables the calculation of the void fraction from known volumetric flow rates of the two phases and this is used in the calculation of the individual components [1]. In the second method, the Friedel correlation [13] is used to estimate the frictional component and the CISE correlation [29] is used to calculate the void fraction from which the accelerational and the gravitational components are estimated. A comparison of the predicted total pressure drop with the

Table 1
Present experimental data on pressure drop

Sl. no.	P (bar)	P_r	G (kg/m^{2}s)	q (kW/m^2)	X_{exit}	ΔP (total) bar
1	10	0.25	1200	35	0.1995	**0.400**
2	15	0.37	1200	35	0.2246	**0.360**
3	20	0.50	1200	35	0.2491	**0.332**
4	25	0.62	1200	35	0.2830	**0.306**
5	30	0.75	1200	35	0.2992	**0.278**
6	32	0.80	1200	35	0.3696	**0.264**
7	34	0.85	1200	35	0.4098	**0.254**
8	36	0.90	1200	35	0.4341	**0.241**
9	38	0.95	1200	35	0.5405	**0.223**
10	10	0.25	1400	35	0.1679	**0.420**
11	15	0.37	1400	35	0.1890	**0.379**
12	20	0.50	1400	35	0.2089	**0.347**
13	25	0.62	1400	35	0.2365	**0.322**
14	30	0.75	1400	35	0.2433	**0.292**
15	32	0.80	1400	35	0.3082	**0.277**
16	34	0.85	1400	35	0.3413	**0.267**
17	36	0.90	1400	35	0.3540	**0.252**
18	38	0.95	1400	35	0.4367	**0.235**
19	10	0.25	1600	35	0.1442	**0.438**
20	15	0.37	1600	35	0.1623	**0.397**
21	20	0.50	1600	35	0.1787	**0.365**
22	25	0.62	1600	35	0.2016	**0.340**
23	30	0.75	1600	35	0.2014	**0.311**
24	32	0.80	1600	35	0.2622	**0.298**
25	34	0.85	1600	35	0.2899	**0.286**
26	36	0.90	1600	35	0.2939	**0.274**
27	38	0.95	1600	35	0.3588	**0.257**
28	10	0.25	1800	35	0.1258	**0.457**
29	15	0.37	1800	35	0.1416	**0.415**
30	20	0.50	1800	35	0.1552	**0.381**
31	25	0.62	1800	35	0.1745	**0.357**
32	30	0.75	1800	35	0.1689	**0.326**
33	32	0.80	1800	35	0.2264	**0.312**
34	34	0.85	1800	35	0.2499	**0.302**
35	36	0.90	1800	35	0.2472	**0.287**
36	38	0.95	1800	35	0.2982	**0.269**
37	10	0.25	2000	35	0.1110	**0.479**
38	15	0.37	2000	35	0.1250	**0.435**
39	20	0.50	2000	35	0.1364	**0.403**
40	25	0.62	2000	35	0.1528	**0.371**
41	30	0.75	2000	35	0.1428	**0.340**
42	32	0.80	2000	35	0.1978	**0.325**
43	34	0.85	2000	35	0.2179	**0.314**
44	36	0.90	2000	35	0.2098	**0.299**
45	38	0.95	2000	35	0.2498	**0.282**
46	10	0.25	1200	60	0.3574	**0.416**
47	15	0.37	1200	60	0.4023	**0.372**
48	20	0.50	1200	60	0.4505	**0.342**
49	25	0.62	1200	60	0.5154	**0.314**
50	30	0.75	1200	60	0.5785	**0.283**
51	32	0.80	1200	60	0.6764	**0.269**
52	34	0.85	1200	60	0.7524	**0.258**
53	36	0.90	1200	60	0.8345	**0.245**
54	38	0.95	1200	60	1.0596	**0.227**
55	10	0.25	1400	60	0.3033	**0.450**
56	15	0.37	1400	60	0.3414	**0.400**
57	20	0.50	1400	60	0.3815	**0.366**
58	25	0.62	1400	60	0.4357	**0.330**
59	30	0.75	1400	60	0.4827	**0.298**
60	32	0.80	1400	60	0.5712	**0.283**
61	34	0.85	1400	60	0.6349	**0.272**
62	36	0.90	1400	60	0.6972	**0.257**
63	38	0.95	1400	60	0.8817	**0.239**

(*continued on next page*)

Table 1 (*continued*)

Sl. no.	P (bar)	P_r	G (kg/m^{2}s)	q (kW/m^2)	X_{exit}	ΔP (total) bar
64	10	0.25	1600	60	0.2627	**0.480**
65	15	0.37	1600	60	0.2957	**0.423**
66	20	0.50	1600	60	0.3297	**0.385**
67	25	0.62	1600	60	0.3760	**0.352**
68	30	0.75	1600	60	0.4109	**0.326**
69	32	0.80	1600	60	0.4923	**0.312**
70	34	0.85	1600	60	0.5468	**0.302**
71	36	0.90	1600	60	0.5943	**0.288**
72	38	0.95	1600	60	0.7482	**0.270**
73	10	0.25	1800	60	0.2311	**0.520**
74	15	0.37	1800	60	0.2601	**0.465**
75	20	0.50	1800	60	0.2894	**0.423**
76	25	0.62	1800	60	0.3295	**0.383**
77	30	0.75	1800	60	0.3551	**0.348**
78	32	0.80	1800	60	0.4310	**0.329**
79	34	0.85	1800	60	0.4783	**0.315**
80	36	0.90	1800	60	0.5142	**0.301**
81	38	0.95	1800	60	0.6443	**0.281**
82	10	0.25	2000	60	0.2058	**0.548**
83	15	0.37	2000	60	0.2317	**0.489**
84	20	0.50	2000	60	0.2572	**0.450**
85	25	0.62	2000	60	0.2923	**0.416**
86	30	0.75	2000	60	0.3104	**0.376**
87	32	0.80	2000	60	0.3819	**0.358**
88	34	0.85	2000	60	0.4235	**0.347**
89	36	0.90	2000	60	0.4501	**0.332**
90	38	0.95	2000	60	0.5613	**0.312**
91	10	0.25	1200	80	0.4838	**0.436**
92	15	0.37	1200	80	0.5445	**0.390**
93	20	0.50	1200	80	0.6116	**0.361**
94	25	0.62	1200	80	0.7014	**0.333**
95	30	0.75	1200	80	0.8019	**0.304**
96	32	0.80	1200	80	0.9219	**0.290**
97	34	0.85	1200	80	1.0265	**0.277**
98	36	0.90	1200	80	1.1549	**0.264**
99	38	0.95	1200	80	1.4750	**0.246**
100	10	0.25	1400	80	0.4116	**0.468**
101	15	0.37	1400	80	0.4633	**0.415**
102	20	0.50	1400	80	0.5195	**0.077**
103	25	0.62	1400	80	0.5951	**0.07**
104	30	0.75	1400	80	0.6742	**0.06**
105	32	0.80	1400	80	0.7816	**0.305**
106	34	0.85	1400	80	0.8699	**0.295**
107	36	0.90	1400	80	0.9718	**0.279**
108	38	0.95	1400	80	1.2376	**0.259**
109	10	0.25	1600	80	0.3574	**0.508**
110	15	0.37	1600	80	0.4023	**0.447**
111	20	0.50	1600	80	0.4505	**0.399**
112	25	0.62	1600	80	0.5154	**0.364**
113	30	0.75	1600	80	0.5785	**0.333**
114	32	0.80	1600	80	0.6764	**0.316**
115	34	0.85	1600	80	0.7524	**0.304**
116	36	0.90	1600	80	0.8345	**0.290**
117	38	0.95	1600	80	1.0596	**0.272**
118	10	0.25	1800	80	0.3153	**0.548**
119	15	0.37	1800	80	0.3549	**0.497**
120	20	0.50	1800	80	0.3968	**0.449**
121	25	0.62	1800	80	0.4534	**0.412**
122	30	0.75	1800	80	0.5040	**0.378**
123	32	0.80	1800	80	0.5946	**0.358**
124	34	0.85	1800	80	0.6610	**0.342**
125	36	0.90	1800	80	0.7277	**0.324**
126	38	0.95	1800	80	0.9212	**0.305**
127	10	0.25	2000	80	0.2816	**0.588**

Table 1 (*continued*)

Sl. no.	P (bar)	P_r	G (kg/m^{2}s)	q (kW/m^2)	X_{exit}	ΔP (total) bar
128	15	0.37	2000	80	0.3170	**0.523**
129	20	0.50	2000	80	0.3538	**0.477**
130	25	0.62	2000	80	0.4039	**0.439**
131	30	0.75	2000	80	0.4444	**0.408**
132	32	0.80	2000	80	0.5292	**0.390**
133	34	0.85	2000	80	0.5879	**0.375**
134	36	0.90	2000	80	0.6423	**0.355**
135	38	0.95	2000	80	0.8105	**0.337**

measured quantity is shown in Fig. 5. It is seen that the homogeneous flow underpredicts the data significantly. The combination of the Friedel correlation for frictional pressure gradient and the Primoli et al. [29] correlation for void fraction appears to work better; however, there is still a consistent underprediction of the data.

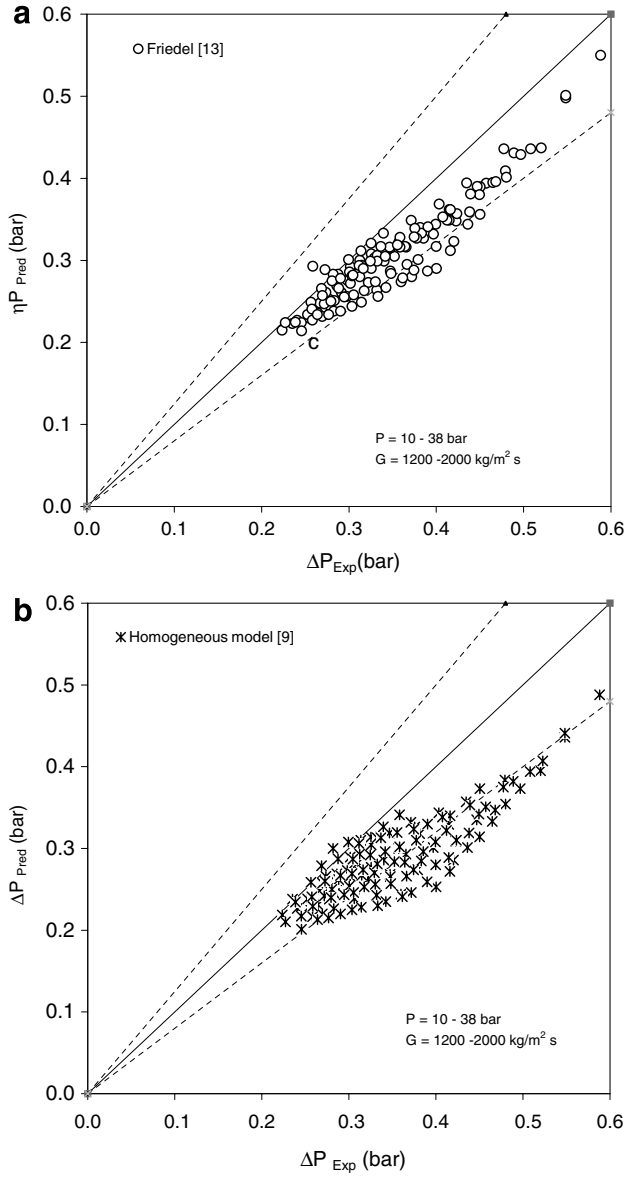

Fig. 5. Comparison of present pressure drop data with predictions from existing methods from literature ([1] and [13]).

The failure of the homogeneous model is not surprising as the properties of the two phases remain significantly different even at very high pressures; it is only at pressures very close to the critical pressure ($P_r > 0.95$) that the thermophysical properties are nearly equal. The failure of the second approach shows that lack of data at high pressures has undermined the accuracy of these purely empirical correlations. In view of this, a third and more rational approach has been used to evaluate the pressure gradient. In this method, the flow pattern map of Hewitt and Roberts [30] is used to first determine the two-flow pattern in each segment based on the segment inlet conditions. In addition to three two-phase flow regimes, namely, bubbly, slug and annular, three other flow regimes, viz., single phase liquid, post-dryout and single phase vapour, are also distinguished. For the sake of convenience, the flow under sub-zero thermodynamic qualities ($x < 0$) is treated as pure single phase liquid; that from the onset of dryout (determined experimentally by the sudden increase in the wall temperature) till the point where the thermodynamic quality is unity is treated as post-dryout regime and the region for which thermodynamic quality is greater than unity is considered as pure vapour flow. It was found from the bulk fluid temperature measurements that the vapour temperature had not risen significantly above the saturation value in the post-dryout regime under the high pressure conditions investigated here. This enables the approximation that the pure vapour flow regime starts at the thermodynamic quality of unity. It may start at much higher thermodynamic qualities if significant vapour superheating takes place in the post-dryout section. But this is likely only at low system pressures [16].

Three volume fractions, namely, continuous liquid, vapour and droplet phase fractions, are evaluated for the three phases. For the pure liquid and pure vapour flow regimes, the corresponding phase fractions are set to unity and the other two are set to zero. For the bubbly flow, the droplet phase fraction is set to zero, the vapour phase fraction is evaluated from the drift flux model [1] and the liquid phase fraction is obtained by difference. For the slug flow regime, the droplet phase fraction is again set to zero and the vapour and the liquid phase fractions are obtained from the slug flow model of Orell and Rembrand [15]. For annular flow, the entrained liquid fraction is determined

from the correlation of Govan [10]. The triangular relationship [31,9] with the Wallis interfacial friction factor correlation [1] is used to obtain the film thickness from which the continuous liquid phase fraction is obtained. From known vapour and entrained droplet mass fluxes, and assuming that the droplets move with the mean vapour velocity, the droplet and the vapour phase fractions are determined. In the post-dryout regime, the continuous liquid phase fraction is set to zero and the droplet phase fraction is assumed once again by assuming no slip between the droplets and the vapour.

Once the volume fractions of each phase are known in each segment, the accelerational and the gravitational components of the pressure drop can be calculated. The frictional component for each regime is calculated in the following way. For single phase liquid or vapour flows, the frictional pressure gradient is obtained from the Blasius relation for turbulent flow through a smooth pipe. For the bubbly and the post-dryout phases, the frictional pressure gradient is estimated from the densities and superficial velocities of the mixture of liquid/bubble or gas/droplet phases, respectively. For the slug flow, the frictional pressure gradient is obtained directly from the Orell and Rembrand model [15] while for the annular flow regime, the frictional pressure gradient is obtained as part of the triangular relationship. The overall set of flow regime criteria and evaluation methods for the phase fraction and the frictional component of the pressure drop are summarized in Table 2.

Typical results from the flow pattern-based pressure drop model are illustrated in Figs. 6 and 7. These show the predicted flow patterns, different pressure drop components and comparison of the overall pressure drop with the experiment for two mass flow rates, three pressures and two heat fluxes. To facilitate the presentation, the data related to the cases of wall heat flux of 35 kW/m^2 are shown in Fig. 6 and those corresponding to the 80 kW/m^2 are shown in Fig. 7. In each figure, the predictions for six different cases are shown; these are:

Case 1: Mass flux = 1200 kg/m^2 s; pressure = 10 bar; $P_r = 0.25$
Case 2: Mass flux = 1200 kg/m^2 s; pressure = 25 bar; $P_r = 0.60$
Case 3: Mass flux = 1200 kg/m^2 s; pressure = 36 bar; $P_r = 0.90$
Case 4: Mass flux = 1800 kg/m^2 s; pressure = 10 bar; $P_r = 0.25$
Case 5: Mass flux = 1800 kg/m^2 s; pressure = 25 bar; $P_r = 0.60$
Case 6: Mass flux = 1800 kg/m^2 s; pressure = 36 bar; $P_r = 0.90$

These six, taken together with the two heat flux values, make it a total of 12 cases for which the predictions are shown in Figs. 6 and 7. For these conditions, four distinct regimes were found to occur: single phase liquid, slug, annular and gas-droplet regimes. The relative length of occurrence of these regimes in the tube in each case is shown in Figs. 6a and 7a. It is seen that as the pressure increases, the length of the subcooled section increases for the same mass and heat fluxes. This rather surprising result is due to the fact that the inlet subcooling is maintained at 3 °C in all cases. As the pressure increases, the latent heat of vapourization decreases rapidly but the specific heat of the liquid increases significantly. Thus an inlet subcooling of 3 °C means close to saturation at low pressures but well below saturation at high pressures. For example, the thermodynamic quality at inlet for Cases 1 and 3 are −1.3% and −10.8%, respectively. The non-boiling length is therefore higher in the latter case. However, the transition through the slug and the annular regions

Table 2
Details of the flow pattern-based model for the pressure drop

Flow regimes	Condition for occurrence flow regime	α_l	α_g	α_d	ΔP_f
Single phase liquid	$x < 0$	1	0	0	From Blasius type friction factor formulae
Bubbly	$0 < x <= x$do and flow pattern map of Hewitt and Roberts [30]	$(1 - \alpha_g)$	From drift flux model	0	Based on mixture velocity
Slug	$0 < x <= x$do and flow pattern map of Hewitt and Roberts [30]	From slug flow model of Orell and Rembrand [14]	From slug flow model of Orell and Rembrand [14]	0	From slug flow model of Orell and Rembrand [14]
Annular	$0 < x <= x$do and flow pattern map of Hewitt and Roberts [30]	From film thickness from triangular relation	$(1 - \alpha_l - \alpha_d)$	From entrained flux assuming drops move at mean vapour velocity	From the triangular relationship with the Wallis interfacial friction factor correlation
Post-dryout	$x$do $< x < 1$	0	$(1 - \alpha_d)$	From entrained flux assuming drops move at mean vapour velocity	Based on mixture properties
Single phase vapour	$x > 1$	0	1	0	From Blasius type friction factor formulae

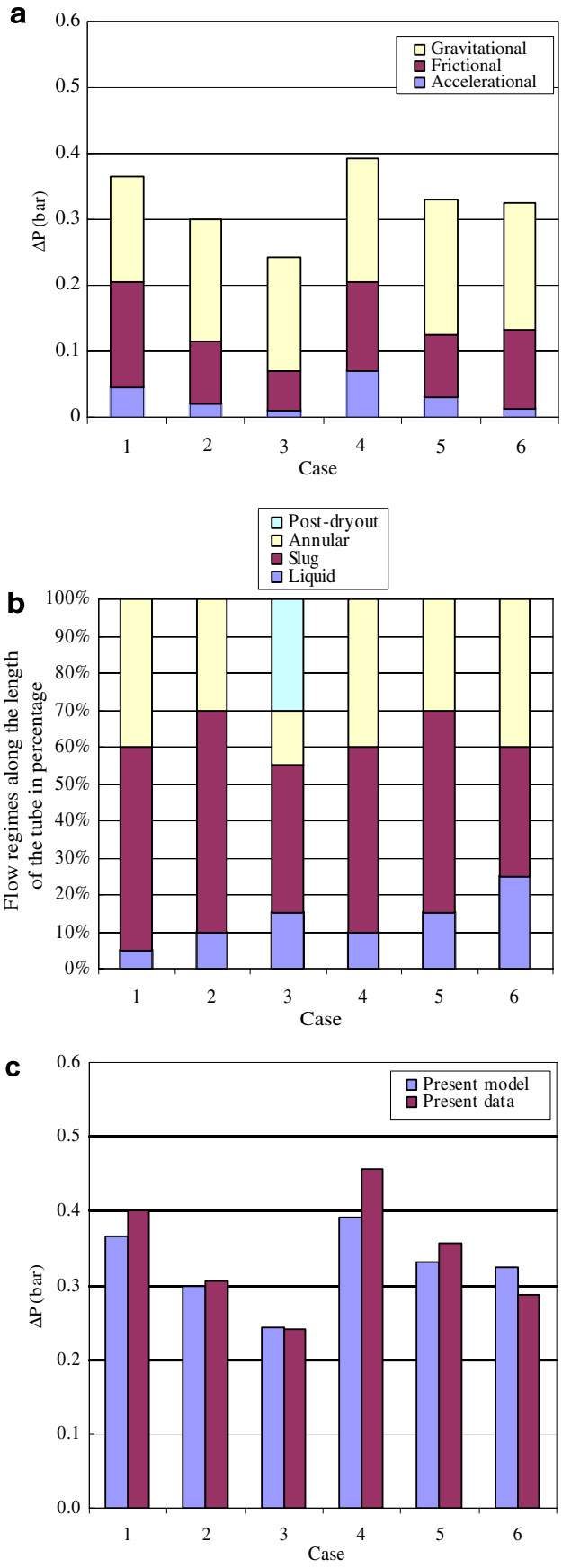

Fig. 6. Typical predictions from flow pattern-based model for $q = 35\ kW/m^2$.

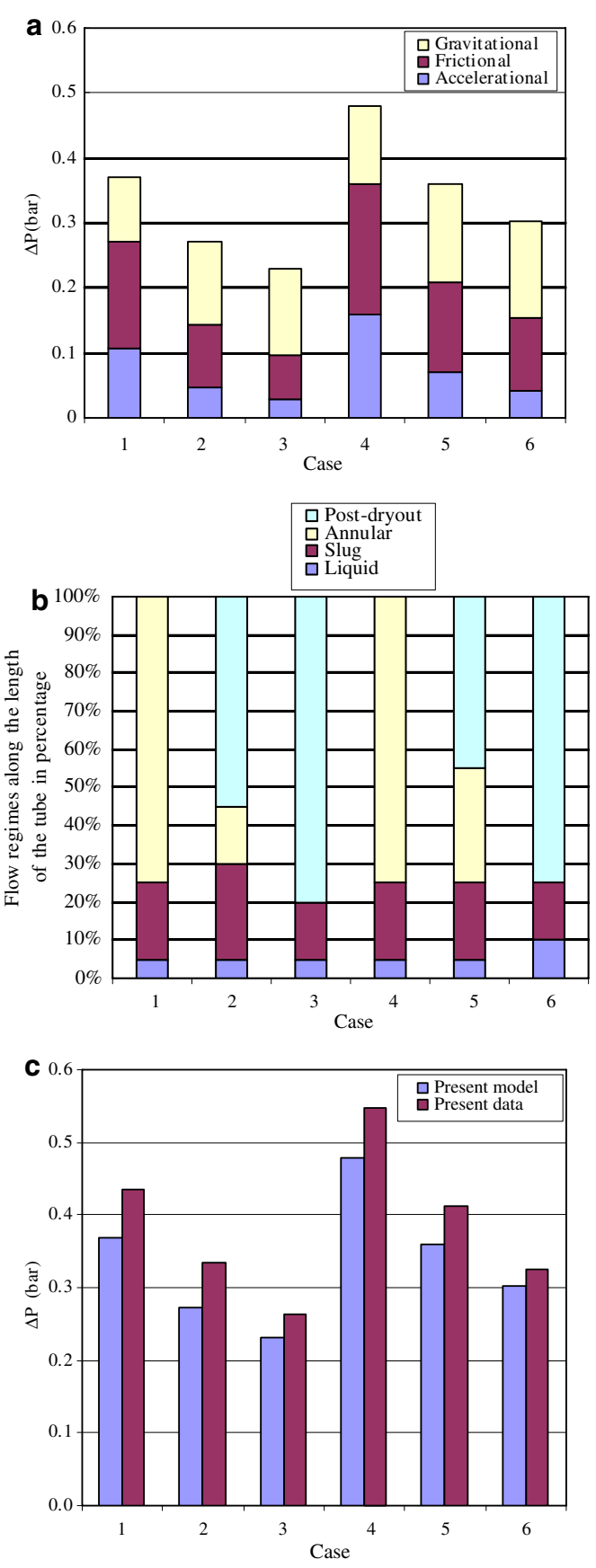

Fig. 7. Typical predictions from flow pattern-based model for $q = 80\ kW/m^2$.

can be more rapid at high pressures. Also, dryout may occur at very low qualities at very high pressures (as can be seen in the experimental data of Becker et al. [32]). Consequently, one may see a wider range of flow patterns at higher pressures. Indeed, the annular flow regime is quite short at high pressures and high mass fluxes and it may be replaced by a gas-droplet flow regime. This may be one of the reasons for the decreased frictional pressure drop at high pressures. Indeed, when this does not happen in Case 6 at a heat flux of 35 kW/m^2 (Fig. 6a), the frictional pressure gradient is found to increase compared with the situation at lower pressures.

Figs. 6b and 7b for the pressure gradient components show that the accelerational component forms only a minor part of the overall pressure drop as the pressure increases. This can be attributed to the fact that the mean vapour phase velocities are much lower at higher pressures due to the very large vapour density. Even though the exit quality is higher (due to decreased latent heat of vapourization), the reduced vapour velocity reduces the overall accelerational component. The gravitational component is more or less the same as the effect of increasing exit quality at higher pressures (resulting in lower gravitational component of pressure drop) is neglected largely by the increased vapour density. As noted above, the frictional component decreases as the pressure increases due to two effects, viz., reduced vapour velocities due to higher density and reduced extent of annular flow due to earlier occurrence of dryout. The overall effect of pressure at constant heat and mass fluxes is therefore to decrease the overall pressure drop.

The comparison between the predicted and the measured pressure drops for the 12 cases is shown in Figs. 6c and 7c. It is seen that fairly good agreement is obtained between the two and the overall trend is captured well. The comparison between the pressure drop predicted by the present flow pattern-based model and the experimental data is shown in Fig. 8 for the entire data set consisting of 135 data points listed in Table 1. Good agreement is obtained between the two with most of the points lying within ±20% of the measured value.

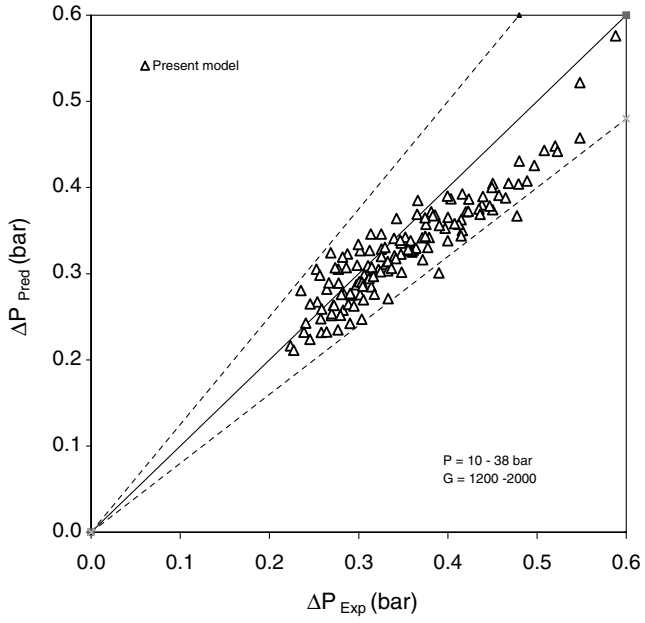

Fig. 8. Comparison of present experimental data with predictions from flow pattern-based model.

5. Conclusions

Experimental data of two-phase pressure drop during flow boiling of R-134a in a vertical tube with internal diameter of 12.7 mm and 3 m length have been obtained in the reduced pressure range of 0.25–0.95; mass flux range of 1200–2000 kg/m^2 s and at constant wall heat fluxes of 35, 60 and 80 kW/m^2 at a constant inlet subcooling of 3 °C. Simultaneous wall and fluid temperature measurements allowed the determination of location of dryout and the subsequent evolution of the vapour temperature. The data show that the overall pressure drop decreases progressively as the system pressure is increased or if the mass flux is decreased.

A flow pattern-based model for the prediction of the pressure drop in the heated tube has been developed. It is based on the division of the tube into several segments, determining the flow pattern in each segment, and use flow pattern-specific methods and correlations to determine the pressure gradient and void fraction within that segment. It is shown that such an approach leads to the satisfactory prediction of the overall pressure gradient in the heated tube.

While detailed validation of the individual components of the models has not been possible, the overall mechanistic approach provides a platform for extension of constitutive relations obtained from essentially low pressure experiments to much higher pressures.

Acknowledgement

The work reported here has been sponsored by the Indian Space Research Organization (ISRO), India.

References

[1] J.G. Collier, Convective Boiling and Condensation, second ed., McGraw-Hill, New York, 1981.
[2] R.W. Lockhart, R.C. Martinelli, Proposed correlation of data for isothermal two-phase, two-component flow in pipes, Chem. Eng. Prog. 45 (1949) 39–48.
[3] O. Baker, Simultaneous flow of oil and gas, Oil Gas J. 53 (1954) 185–190.
[4] A.E. Dukler, Y. Taitel, Flow pattern transitions in gas–liquid systems, measurement and modeling, in: G.F. Hewitt, J.M. Delhaye, N. Zuber (Eds.), Multiphase Science and Technology, vol. 2, Begell House, New York, 1986, pp. 1–94 (Chapter 1).
[5] R.C. Fernandes, R. Semiat, A.E. Dukler, Hydrodynamic model for gas–liquid slug flow in vertical tubes, AIChE J. 29 (1983) 981–989.

[6] A.E. Dukler, M.G. Hubbard, A model for gas–liquid slug flow in horizontal and near horizontal tubes, Ind. Eng. Chem. Fundam. 14 (1975) 337–346.
[7] N.D. Sylvester, A mechanistic model for two-phase vertical slug flow in pipes, Trans. ASME 109 (1987) 206–213.
[8] P.B. Whalley, Boiling, Condensation and Gas–liquid Flow, Clarendon Press, Oxford, 1987.
[9] G.F. Hewitt, A.H. Govan, Phenomenological modeling of non-equilibrium flows with phase change, Int. J. Heat Mass Transfer 33 (1990) 229–242.
[10] D. Chisholm, L.A. Sutherland, Prediction of pressure gradients in pipeline systems during two-phase flow, Proc. Instn. Mech. Engrs. 184 (Pt 3C) (1969–70) 24–32.
[11] B. Chexal, G. Lellouche, J. Horowitz, J. Healzer, A void fraction correlation for generalized applications, Progr. Nuclear Energy 27 (1992) 255–295.
[12] L. Friedel, Improved friction pressure drop correlations for horizontal and vertical two-phase pipe flow, European two-phase Group Meeting, Ispra, Italy, Paper E2, June 1979.
[13] D. Chisholm, Pressure gradients due to friction during the flow of evaporating two-phase mixtures in smooth tubes and channels, Int. J. Heat Mass Transfer 16 (1973) 347–358.
[14] A. Orell, R. Rembrand, A model for gas–liquid slug flow in a vertical tube, Ind. Eng. Chem. Fundam. 25 (1986) 196–206.
[15] N. Hoyer, Calculation of dryout and post-dryout heat transfer for tube geometry, Int. J. Multiphase Flow 24 (1997) 319–334.
[16] S. Jayanti, M. Valette, Prediction of dryout and post-dryout heat transfer at high pressures using a one-dimensional three-fluid model, Int. J. Heat Mass Transfer 47 (2004) 4895–4910.
[17] T.N. Tran, M.C. Chyu, M.W. Wambsganss, D.M. France, Two-phase pressure drop of refrigerants during flow boiling in small channels: and experimental investigation and correlation development, Int. J. Multiphase flow 26 (2000) 1739–1754.
[18] T.N. Tran, M.W. Wambsganss, D.M. France, Small circular and rectangular channel boiling with two refrigerants, Int. J. Multiphase Flow 22 (1996) 485–498.
[19] M. Zhang, R.L. Webb, Correlation of two-phase friction for refrigerants in small diameter tubes, Exper. Therm. Fluid Sci. 25 (2001) 131–139.
[20] W. Yu, D.M. France, M.W. Wambsganss, J.R. Hull, Two phase pressure drop, boiling heat transfer, and critical heat flux to water in a small-diameter horizontal tube, Int. J. Multiphase Flow 28 (2002) 927–941.
[21] S.M. Sami, J.D. Comeau, Influence of thermophysical properties on two-phase flow convective boiling of refrigerant mixtures, Appl. Therm. Eng. 22 (2002) 1535–1548.
[22] G.R. Warrier, V.K. Dhir, L.A. Momoda, Heat transfer and pressure drop in narrow rectangular channels, Exper. Therm. Fluid Sci. 26 (2002) 53–64.
[23] F. Fu, F. Klausner, A separated flow model for predicting two-phase pressure drop and evaporative heat transfer for vertical annular flow, Int. J. Heat Fluid Flow 18 (1997) 541–549.
[24] W. Tong, A.E. Bergles, M.K. Jensen, Pressure drop with highly subcooled flow boiling in small diameter tubes, Exper. Therm. Fluid Sci. 15 (1997) 202–212.
[25] T.S. Zhao, Q.C. Bi, Pressure drop characteristics of gas–liquid two-phase flow in vertical miniature triangular channels, Int. J. Heat Mass Transfer 44 (2001) 2523–2534.
[26] S.W. Churchill, Frictional equations spans all fluid flow regimes, Chem. Eng. 84 (1977) 91–92.
[27] Ing Youn Chen, Kai-Shing Yang, Chi-Chung Wang, An empirical correlation for two-phase frictional performance in small diameter tubes, Int. J. Heat Mass Transfer 45 (2002) 3667–3671.
[28] D.S. Wen, D.B.R. Kenning, Two phase pressure drop of water during flow boiling in a vertical narrow channel, Exper. Therm. Fluid Sci. 28 (2004) 131–138.
[29] A. Premoli, D. Francesco, A. Prina, An experimental correlation for evaluating two-phase mixture density under adiabatic conditions, European Two-Phase Flow Group Meeting, Milan, 1970.
[30] G.F. Hewitt, D.N. Roberts, Studies of two-phase flow patterns by X-ray and flash photography, AERE-M 2159.H.M.S.O., 1969.
[31] G.F. Hewitt, N.S. Hall-Taylor, Annular Two-phase Flow, Pergamon Press, Oxford, UK, 1970.
[32] K.M. Becker, C.H. Ling, S. Hedberg, G. Strand, An experimental investigation of post dryout heat transfer, Department of Nuclear Reactor Engineering, Royal Institute of Technology report KTH-NEL-33, Stockholm, Sweden, 1983.